

An exploratory study of stress wave communication in concrete structures

Qing Ji¹, Michael Ho², Rong Zheng³, Zhi Ding⁴ and Gangbing Song^{*1,2}

¹Department of Electrical Engineering, University of Houston, Houston, TX, USA

²Department of Mechanical Engineering, University of Houston, Houston, TX, USA

³Department of Computing and Software, McMaster University, Hamilton, ON, Canada

⁴Department of Electrical Engineering, University of California, Davis, Davis, CA, USA

(Received January 9, 2014, Revised May 10, 2014, Accepted May 25, 2014)

Abstract. Large concrete structures are prone to cracks and damages over time from human usage, weathers, and other environmental attacks such as flood, earthquakes, and hurricanes. The health of the concrete structures should be monitored regularly to ensure safety. A reliable method of real time communications can facilitate more frequent structural health monitoring (SHM) updates from hard to reach positions, enabling crack detections of embedded concrete structures as they occur to avoid catastrophic failures. By implementing an unconventional mode of communication that utilizes guided stress waves traveling along the concrete structure itself, we may be able to free structural health monitoring from costly (re-)installation of communication wires. In stress-wave communications, piezoelectric transducers can act as actuators and sensors to send and receive modulated signals carrying concrete status information. The new generation of lead zirconate titanate (PZT) based smart aggregates cause multipath propagation in the homogeneous concrete channel, which presents both an opportunity and a challenge for multiple sensors communication. We propose a time reversal based pulse position modulation (TR-PPM) communication for stress wave communication within the concrete structure to combat multipath channel dispersion. Experimental results demonstrate successful transmission and recovery of TR-PPM using stress waves. Compared with PPM, we can achieve higher data rate and longer link distance via TR-PPM. Furthermore, TR-PPM remains effective under low signal-to-noise (SNR) ratio. This work also lays the foundation for implementing multiple-input multiple-output (MIMO) stress wave communication networks in concrete channels.

Keywords: SHM; stress wave communication; smart aggregate; time reversal; PPM; TR-PPM

1. Introduction

Concrete structures have been extensively used for over a century. However, in recent years, many such structures have aged and deteriorated to the point of structural failure, sometimes causing collapse-related accidents in many parts of the world. The problem of aging infrastructure highlights the importance of concrete structural health monitoring (SHM). With an increased focus on structural integrity to meet safety regulations, there is an acute need for real-time updates on

*Corresponding author, Professor, E-mail: gsong@uh.edu

health status of concrete structures, with continuous recording and data export throughout the life cycle. Structural health monitoring (SHM) related techniques provide an innovative potential to improve operational safety of concrete structures while cutting down installation and maintenance expenses. Recently, wireless sensor networks (WSNs) based structure health monitoring have attracted increasing attention owing to their low cost and ease of installation over conventional monitoring systems that relying on piezoelectric sensors wired to a personal computer (PC), (e.g., Li *et al.* 2010). Although optimized power system design and intelligent sleep management can increase the lifetime of WSN SHM systems (e.g., Li *et al.* 2010), the need for battery replacement remains still a key challenge for many civil applications (Hoult *et al.* 2009). Furthermore, for structures buried underground or submerged in water, it is difficult and often infeasible to use wireless RF communication.

Piezoelectric based smart aggregate (SA) has proven to be effective both as sensors and actuators, further enhancing its multi-functionality in concrete SHM, including early age strength monitoring, impact detection and structural health monitoring (Song *et al.* 2008). Additionally, smart aggregates can be employed for energy harvesting from ambient vibration and long distance energy charging by focusing techniques. For these reasons, it is natural and desirable to develop a fully autonomous SHM system capable of damage detection, health monitoring, self powering, and wire-free communication via the host concrete structure itself as the channel medium.

Low power, long range stress wave communication propagating within the concrete structure is a very attractive solution. Thus far, works on stress wave data communication in the structures are rather limited. Several research teams have investigated ultrasonic digital communication through metallic structures (e.g., Graham *et al.* 2009, Primerano 2010, Murphy 2006), though systematic data communication schemes remain unclear. Kokossalakis (2006) proposed using underwater pipelines as an acoustic waveguide for modulated wave transmission. Frequency-shift keying (FSK), amplitude-shift keying (ASK) and quadrature amplitude modulation (QAM) methods are shown to have similar bit error performance. Several signal processing steps were proposed to compensate for channel dispersion. Johnson (1972) tested seismic communications with a data rate of two pulses per second at a distance of 760 ft through hard rocks by using an impedance matched piezoelectric transducer as the transmitter. Jin *et al.* (2011) developed a time reversal based guided elastic wave communication scheme that utilizes steel pipes as transmission channels for structural health monitoring applications. Kailaswar *et al.* (2012) proposed a single-input single-output (SISO) communication paradigm using cement-based SA embedded concrete channel based on the D8PSK modulation scheme. They observe that multipath is not rich in concrete medium. Although the concrete medium is mostly homogeneous, the new generation marble-based SA that consists of a piece of lead zirconate titanate (PZT) patch sandwiched between a pair of marble blocks through epoxy (Hou *et al.* 2012), contributes to the inhomogeneous channel environment for wave propagation. According to Snell's law, as the stress wave passes the border between media, the wave is reflected at the interface and also refracted at an angle that depends upon the relative refractive indices of the two media. Marble-based SAs are more stable in mechanical performance compared with cement-based SAs. Hence, when applying marble-based SA for structure health monitoring, a communication scheme is required to overcome the signal delay spread caused by multipath channels. Furthermore, for future consideration of multiple-input multiple-output (MIMO) communication links that utilize stress waves propagating through concrete over the distances for structural health monitoring, diverse multipath dispersion across various transmit-receive paths can provide the useful MIMO channel gain and MIMO capacity. This channel diversity in MIMO system (e.g., Sharony 2006) can take advantage of the dispersive

effects generated by inhomogeneous media for multiple-channel and simultaneous multi-sensor transmission over the same concrete channel. With this understanding, a communication scheme is needed to also overcome the resulting multipath distortion when taking advantage of the multipath for MIMO communications.

More recently, there has been substantial interest in ultra-wide band (UWB) communications because of its potentially low complexity and low power. Among others, pulse position modulation (PPM) modulation offers notable advantage with respect to power efficiency (Ramirez-Iniguez *et al.* 2008). In this paper, we develop a novel method of PPM inside concrete using stress wave communications. To mitigate distortions due to multipath channel dispersion, we propose a time reversal based pulse position modulation (TR-PPM) for single channel (SISO) stress wave transmission and reception. Our work contributes to the foundation for future implementation of MIMO stress wave communications.

2. Theoretical basics and discussion

2.1 Channel response and stress wave propagation using different SAs

Two generations of SAs have been developed for structural health monitoring. For the 1st generation, the PZT patch is embedded within a concrete block (Gu *et al.* 2006), whereas the 2nd generation PZT patch is sandwiched between marble blocks. Piezoelectric materials can generate electric charge in response to applied mechanic forces and can produce stress or strain when subjected to an electric field. Under an alternating potential difference, the material is set to elastic vibration, which produces stress waves.

In order to take full advantage of different SA properties for stress wave communication in concrete blocks, it is necessary to characterize channel response when different SAs are embedded into the concrete specimen. Thus, two concrete cylinder specimens (radius: 3", height: 12") are set up as shown in Fig. 1. The details of composition and properties of the concrete are presented in Tables 1 and 2.

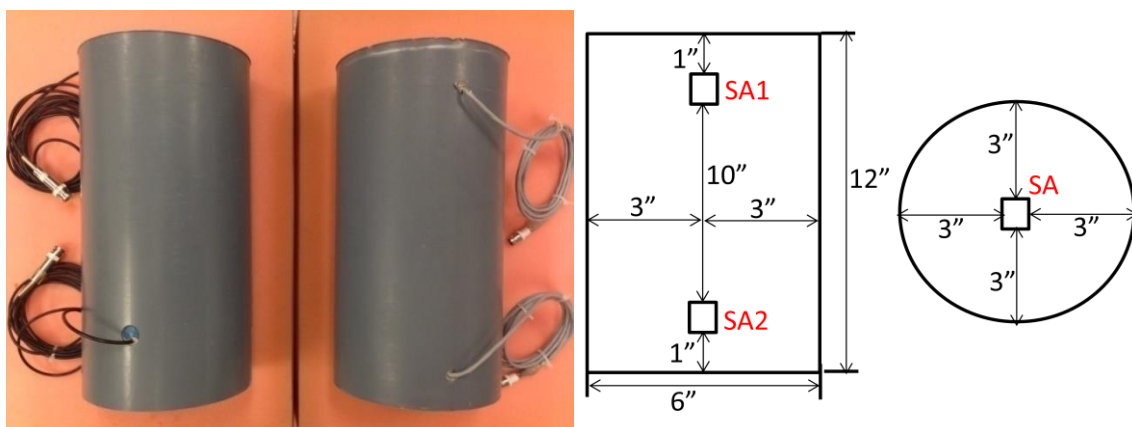


Fig. 1 Two concrete cylinder specimens with different SAs and Diagram for SA locations

Table 1 Compositional details of the concretes

Component	Composition(kg/m ³)	Description
Cement	340	Type I-Portland cement
Sand	700	Standard sand
Coarse aggregate	1125	½ inch size angular limestone
Water	200	Tap water

Table 2 Properties of 28-day fully cured concretes

Physical parameters	Values
Density (kg/m ²)	2400
Young's Modulus (MPa)	32000
Poisson ratio	0.2

One cylinder is embedded with marble-based SAs embedded while the other is embedded with cement-based SAs. A 10mm thickness sponge sheet under the cylinders isolates wave propagation. For each concrete cylinder, piezoelectric actuator and the piezoelectric sensor, in the form of SAs, are positioned along the central axis of the cylinder specimen, separated by a distance of 10 inches. The tests were carried out when concrete cylinders have fully cured for 28 days.

Here we employ the least-squares (LS) method which is a widely used for channel estimation. The received signal $y(t)$ can be expressed in terms of a linear time-invariant system as follows

$$y(t) = x(t) \otimes f(t) + v(t) \quad (1)$$

where \otimes denotes the linear convolution operation, $f(t)$ is the channel impulse response, $x(t)$ is the transmitted signal, and $v(t)$ denotes the noise.

After sampling with sampling frequency F_s , the discrete-time version of received signal is

$$y = Xf + v \quad (2)$$

where $f = [f_0 \ f_1 \ \dots \ f_{M-1}]^T$ and $x = [x_0 \ x_1 \ \dots \ x_{M+N-1}]^T$. The transmitting signal is divided into a reference length of N and guard period of M bits, and M is the channel memory. The Toeplitz

matrix $X \in \mathbb{C}^{N \times M}$ is formed as $X =$

$$\begin{bmatrix} x_{M-1} & \cdots & x_1 & x_0 \\ x_M & \cdots & x_2 & x_1 \\ \vdots & & \cdot & \vdots \\ x_{M+N-2} & \cdots & x_N & x_{N-1} \end{bmatrix}$$

The LS channel estimate is found by minimizing the following squared-error function

$$\hat{f} = \arg \min_f \|y - Xf\|^2 \tag{3}$$

which gives the LS solution $\hat{f}_{LS} = (X^H X)^{-1} X^H y$, Where $()^H$ and $()^{-1}$ denote the Hermitian and inverse matrices, respectively.

In the experiment, for both specimens, the actuator SA1 emits the Gaussian white noise signal and the sensor SA2 receives the transmitted stress wave from SA1. Fig. 2 shows the LS channel estimation results in two different specimens. The concrete channel using marble-based SAs has better response in high frequencies around 80 KHz while the channel using cement-based SAs has better response in relative low frequencies.

For cylindrical concrete structures, stress waves can be generally categorized into three families, namely the torsional (T), longitudinal (L) and flexural (F) waves. There exist several different guided wave modes in each family. Guided stress waves are known to be dispersive because the wave mode velocity varies with its frequency. The changes in phase velocity with respect to frequency are simulated for the concrete used in the experiments (Fig. 3) using software GUIGUW (Bocchini *et al.* 2011). While the fundamental mode (L (0, 1), T (0, 1), F (1, 1)) is defined over the entire frequency range, the branches of higher modes started to propagate at their cut-off frequency. The cut-off frequencies of higher modes start from around 20 KHz. The number of wave modes increases as the frequency increases. Higher frequency signals excite more propagation modes. The fundamental torsional mode T (0, 1) is non-dispersive while the other modes are highly dispersive, especially at their respective low frequencies. In other words, a small change in frequency causes a relatively large velocity change at low frequency. It is this non-constant channel group delay that causes frequency dispersion. For each mode, as the frequency increases, the level of dispersion decreases. In particular, a pulse may contain a wide range of frequencies and potentially excites many modes. Since the concrete channel using cement-based SAs acts as a low pass filter, only the fundamental modes are excited and the channel appears less dispersive.

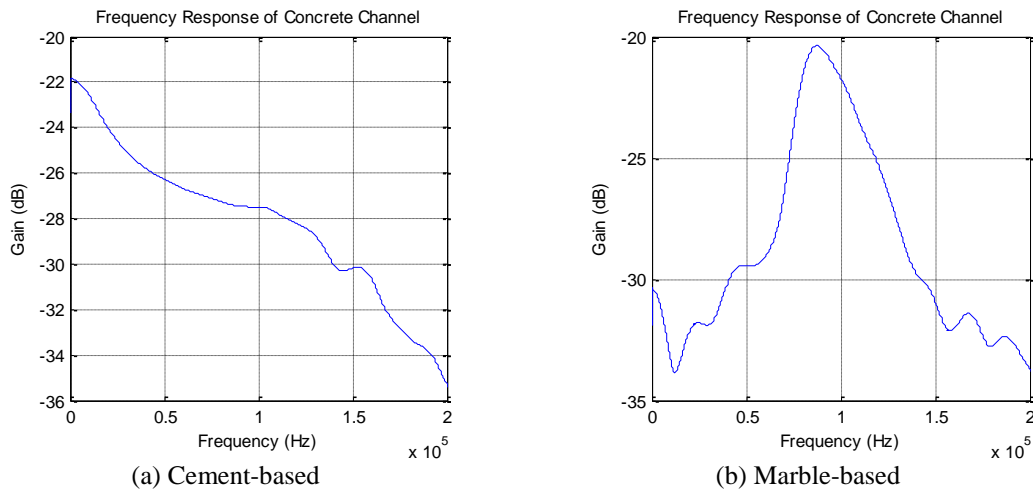


Fig. 2 Frequency response of two different cylinder specimens

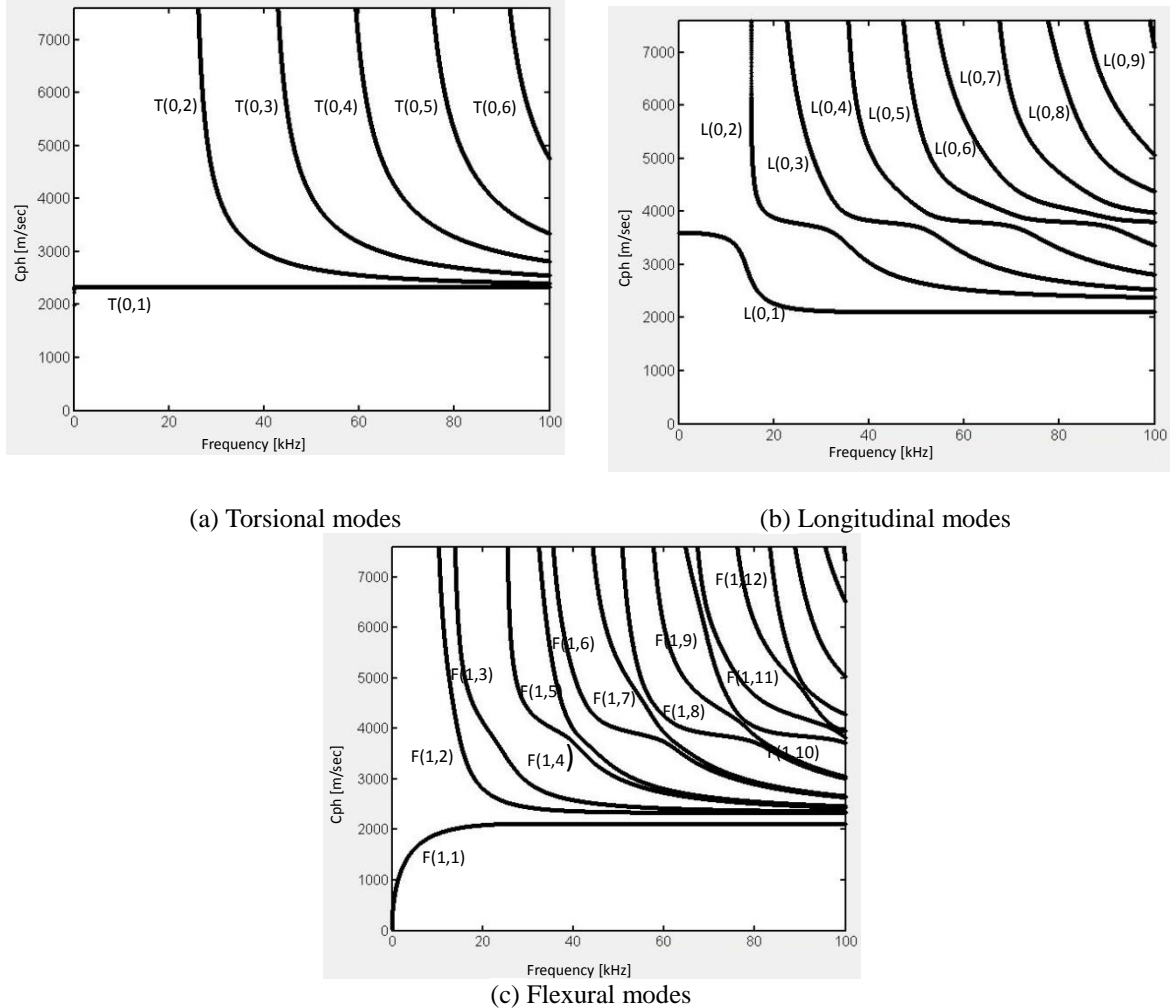


Fig. 3 Phase speed versus frequencies dispersion curves

The concrete channel using marble-based SAs has a good high-frequency response, and the channel becomes more dispersive as more modes are stimulated. As a result, a pulse signal traveling through the concrete becomes heavily distorted when using the marble SAs. On one hand, the multipath diversity may be potentially exploited by properly designed modulation schemes in multi-antenna systems. On the other hand, the communication system must also compensate for Inter-Symbol Interference (ISI) due to channel dispersion.

2.2 Principle of time reversal communication

In order to combat severe channel dispersion, we adopt time reversal communication utilizing the stress wave. The spatial and temporal focusing property of time reversal can take advantage of the dispersion caused by the channel by applying matched pulse-shape to focus multipath energy

for increasing received SNR. Time reversal technique has been applied under dispersive channels in many applications, including defects detection in pipes (e.g., Ying *et al.* 2010), underwater acoustics (e.g., Edelmann *et al.* 2005), electromagnetic (e.g., Jin *et al.* 2007), and stress wave communication, etc..

Consider an input signal $x(t)$ generated by SA1. Let $f(t)$ represent the corresponding impulse response function, then, $y(t)$ received by the SA2 can be written as

$$y(t) = x(t) \otimes f(t) \quad (4)$$

where \otimes denotes the convolution operation.

The received signal at SA2 is reversed in time, namely time reversal signal $y(-t)$

$$y(-t) = x(-t) \otimes f(-t) \quad (5)$$

When the time reversed signal is sent from SA2 to SA1, assuming the channel is reciprocal, the received signal can be given as

$$y^{TR}(t) = y(-t) \otimes f(t) = x(-t) \otimes [f(-t) \otimes f(t)] = x(-t) \otimes [f(t) \odot f(t)] \quad (6)$$

where \odot denotes time correlation.

Most of input signals are time reversal symmetric, such as Gaussian pulse, sinusoidal signals, and square signals, i.e., $x(-t)=x(t)$. Therefore, the received signal is a convolution of input signal and an autocorrelation function which is often called the time reversal operator. The operator named $g^{TR}(t)$, is represented as

$$g^{TR}(t) = \int_{-\infty}^{\infty} f(\tau) f(\tau - t) d\tau \quad (7)$$

From Eq. (7), it is shown that the time reversal operator is an even function. Therefore the received signal is always time reversal symmetric in the time domain. When $t=0$, time reversal operator has the maximum value

$$g^{TR}(0) = \int_{-\infty}^{\infty} f^2(\tau) d\tau \quad (8)$$

This proves that the received signal $y^{TR}(t)$ is a time reversal symmetric focusing signal.

2.3 Design of PPM and TR-PPM communication

Fig. 4 illustrates the basic diagram of the (TR-) PPM transmitter in which the pulse-shaper can executive TR-PPM by adopting the time-reversed waveform it received from its partner node. This transmitter consists of the following components:

1. The binary source provides in binary format the information $a = (a_1, a_2, a_3, \dots, a_j)$ that the stress wave needs to deliver.
2. Transmission coder applies an integer-value code $c = (c_1, c_2, c_3, \dots, c_j)$ to the binary sequence a and generates a new sequence d expressed as follows: $d_j = c_j T_c + a_j \varepsilon$, where c_j is the time hopping code which plays the role of code division multiple access for multiple users, and T_c is the chip time. ε represents the time shift specified on the given chip block and

$a_j \varepsilon$ is the symbol duration introduced by the PPM which depends on the bit to be represented. In this paper, we used the basic PPM modulation scheme, that is $c_j = 0$

3. PPM Modulator generates a sequence of unit impulses which are located at times $jT_s + d_j$.
4. Pulse shaper functions as a filter with impulse response $p(t)$.
 - a. For the conventional PPM method, it can be the Gaussian modulated sine waveform

$$p(t) = Ae^{-k(i*\Delta t)^2} \cos(2\pi f_c(i*\Delta t))$$

$$k = \frac{5\pi^2 b^2 f_c^2}{q * \ln(10)} \text{ for } i = 0, 1, 2, \dots, N-1,$$

Where A is the amplitude, b is the normalized bandwidth, q is the attenuation, f_c is the center frequency (Hz), d is the delay, and N is the samples.

- b. For the TR-PPM method, $p(t) = kr(-t)$ where $r(t)$ is the channel impulse response, $r(-t)$ is the time reversed channel response waveform. The transmitting TR-PPM

modulated signal takes the form of $s(t) = \sum_{j=-\infty}^{+\infty} kr(-t)\delta(t - jT_s - c_j T_c - a_j \varepsilon)$

3. Experimental setup and channel analysis

3.1 Experimental setup for PPM and TR-PPM communication experiment

The experimental setup (Fig. 5) includes a concrete block of dimension 72''x5''x3'' with multiple marble-based SAs embedded inside. The concrete block was casted with the exactly the same parameters as the cylinder's casting (shown in Table 1) and all the experiments were conducted when concrete block has fully cured for 28 days. An NI USB X Series 6361 Data Acquisition System interfaced with a laptop through LabVIEW software collects data, while a PZT amplifier boosts signal transmission. The maximum input sampling rate of data acquisition system is 2 MHz per channel and the input/output dynamic range is [-10V, 10V]. The data acquisition system sent a signal through the analog output port to a PZT amplifier. The amplified signal excites one of the SAs (as the actuator) in concrete. The vibrating signal propagated through the concrete, and is received by the other SA (as the sensor). The analog input port of the data acquisition system sensed the SA vibration and acquired the received waveform for information extraction and decoding.

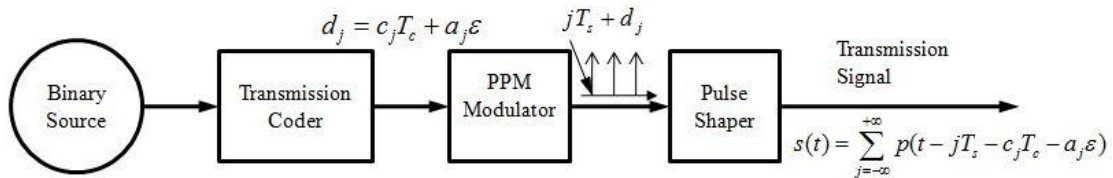


Fig. 4 PPM and TR-PPM transmission scheme

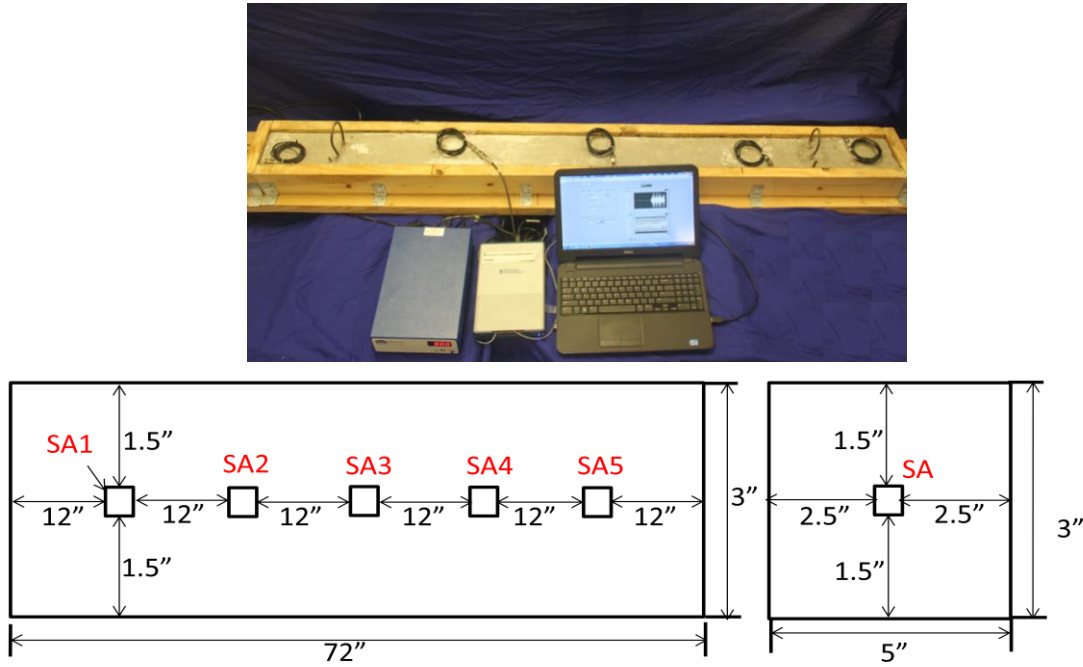


Fig. 5 Experimental setup and Diagram for SA locations

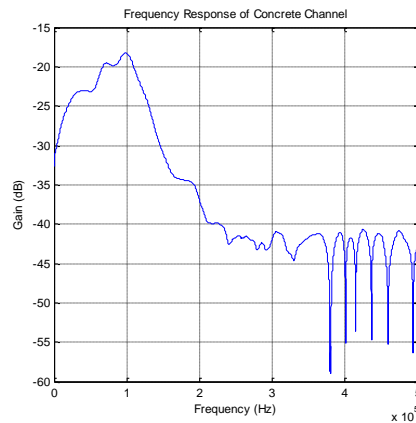


Fig. 6 Frequency response for concrete block channel

3.2 Channel response and dispersion curves

Using the same LS channel estimation method as section 2.1, we get very similar concrete channel responses between different SAs. As an example, the channel response between SA2 and SA3 is shown in Fig. 6. We observe that the channel gain increases exponentially before 10 KHz and has a steeper roll-off after 100 KHz. Concrete channel achieves its best response around 100 KHz.

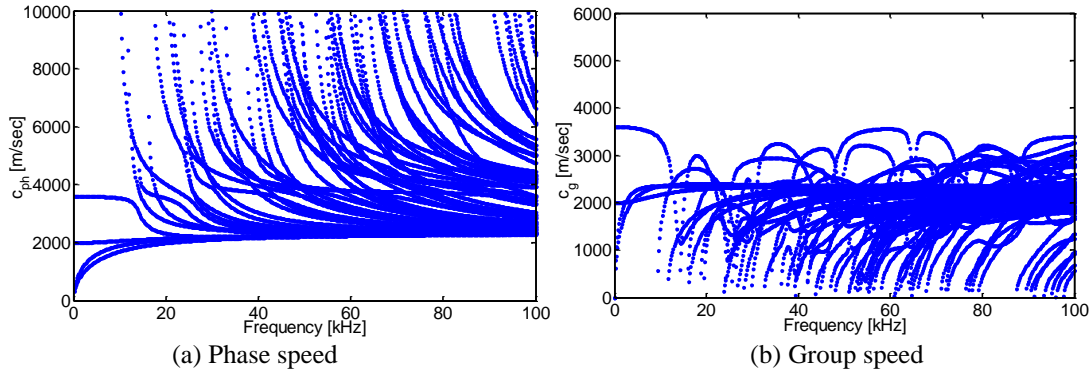


Fig. 7 Dispersion curves for concrete block specimen

Besides, the dispersion curve in the concrete block is simulated by GUIGUW in Fig. 7. Similar to the simulation results using cylinder model, different modes travel with different phase speeds. Also, based on the group dispersion curves, it is noted that energy carried by different modes is transmitted in different velocity which is consistent with the phase dispersion.

4. Experimental procedures

We use the stress wave communication between SA2 and SA3 as an example to describe the following steps in the experiments.

1. Selection of a concrete channel resonance frequency as the center frequency for modulated Gaussian pulse $p(t) = Ae^{-k(i*\Delta t)^2} \cos(2\pi f_c(i*\Delta t))$. In digital communication systems, it is well known that if the frequency response of the channel changes significantly within the band of the transmitted signal, the modulated signal going through the channel will be distorted, resulting in ISI. Excluding the relatively steep frequency response part, the frequency range between 10 KHz and 100 KHz for the Gaussian pulse is selected to conduct trial-and-error experiments. After a lot of trials, we choose a Gaussian modulated sine wave with 50.7 KHz center frequency and bandwidth 80 KHz which is shown in Fig. 8 for optimal performance.

2. Transmission of a modulated Gaussian pilot signal and measuring channel response between two SAs. Fig. 9 shows received signal from SA3 when SA2 transmits a modulated Gaussian pulse at center frequency of 50.7 KHz. The modulated Gaussian pulse waveform experiences substantial dispersion after traveling through the concrete. This severe time spreading response results from channel multipath and dispersion of stress waves.

3. Reversal of normalized sounding signal and feedback: The channel sounding signal is time reversed (Fig. 10) and amplitude normalized (maximum amplitude value was scaled to 500V) in order to get the best SNR improvement, and then is retransmitted back to the same channel. The received signal is a focused signal (Fig. 11) with a distinct peak, indicating that most energy from different wave modes arrive at the receiver simultaneously. This peak allows for accurate synchronization and signal decoding when transmitting data streams. The reversed channel response waveform is used to replace each pulse when modulating the data information in step 4.

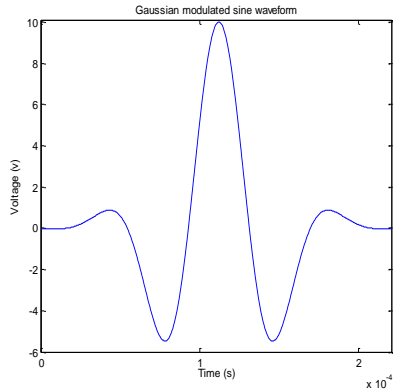


Fig. 8 Gaussian modulated sine waveform

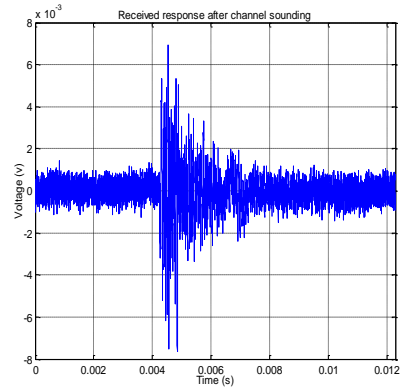


Fig. 9 Channel response (SA2, SA3)

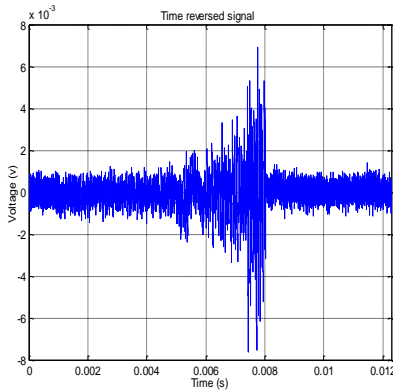


Fig. 10 Time reversed signal (SA2, SA3)

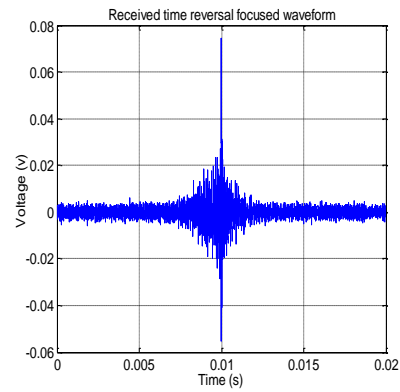


Fig. 11 Received time reversal focused waveform (SA2, SA3)

4. Transmission and reception of modulated time reversal signals to the SA2 after encoding a stream of binary bits. The binary streams are encoded through relative pulse shift within each data frame based on the time reversed channel response signal. The experiments are tested out at the data rates of 200 bps, 500 bps and 1 Kbps, respectively. The maximum amplitude value of output waveforms from the analog output port, which is the input of the amplifier, is scaled to the same value at all times for fair comparison between PPM and TR-PPM communication methods.

5. Experimental results

Conventional PPM and TR-PPM communication experiments are each carried out between different SA pairs under multiple transmission data rates of 200 bps, 500 bps, and 1 Kbps. The following sub-sections compare the results between the two different communication schemes under three transmission data rates in three different scenarios: short range communication, low signal-to-noise ratio (SNR) communication and relatively long distance communication.

5.1 Short range stress wave communication experiments via PPM and TR-PPM

Fig. 12 shows the experimental results at three different data rates between the nearest SA pairs (SA2 and SA3) transmitting the bit stream [1101010011]. The amplifier connected to the SA2 (as actuator) outputs the excitation signal of peak amplitude value 500V. The received information-bearing waveforms encoded by two different modulation communication methods are compared. SA3 received the decodable waveforms for both PPM and TR-PPM at data rate of 200 bps. For PPM communications, the received waveform becomes harder to discern (or demodulate) at 500 bps and actually fails to show signal peaks at 1 Kbps because of the severe signal dispersion. However, TR-PPM communication results clearly show focusing peaks at both 500 bps and 1 Kbps data rates. We notice that there are several weak peaks at data rates of 500 bps and 1 Kbps due to ISI. As the data transmission rate grows, the ISI becomes more significant. We conclude that transmitted stress wave signals can be decoded better according to the clearly visible signals peaks in TR-PPM at higher data transmission rate.

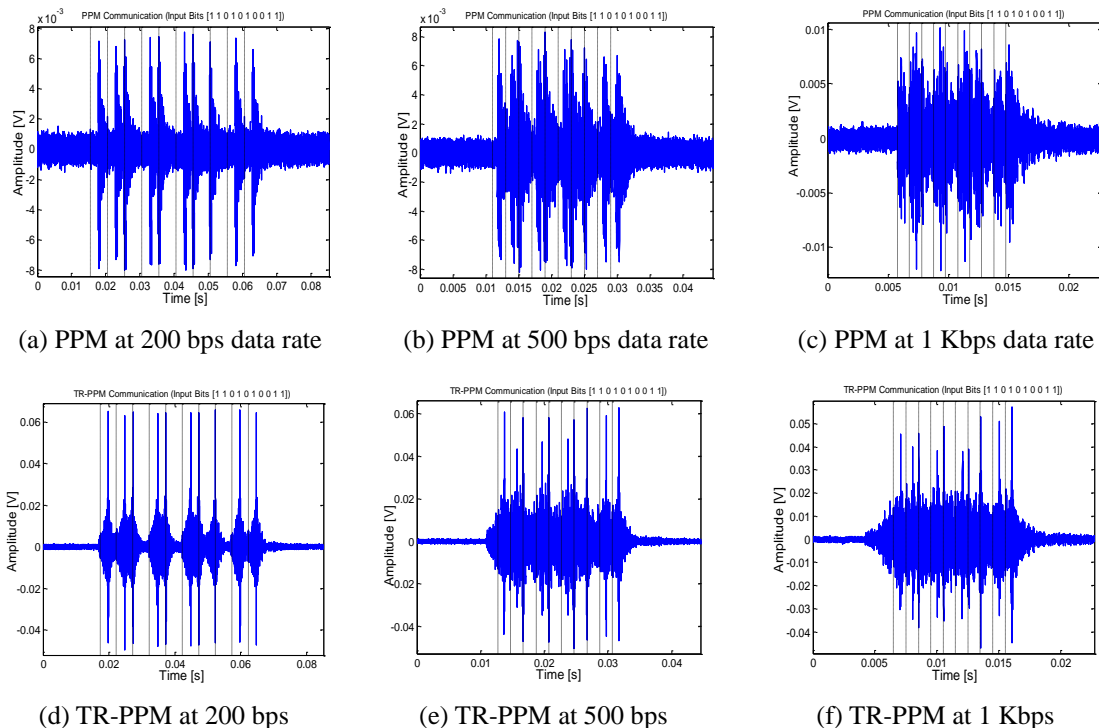


Fig.12 PPM and TR- PPM communication between SA2 and SA3 with bit stream [1101010011]

5.2 Low SNR stress wave communication experiments via PPM and TR-PPM

To further evaluate the link performance at low SNR, we reduce the maximum amplitude value of the modulated signal to 25V without changing the main experimental settings (using SA2 and SA3). Similar to the previous experiment, PPM and TR-PPM communication are tested and compared in three different data rates (Fig. 13). Comparing their received signals in Fig. 10, it is clear that the SNR is lower given the reduced excitation signal. For PPM, the received signal is fully submerged in noise and undetectable due to the low SNR for all three data rates cases. But TR-PPM demonstrates robustness in low SNR conditions and the advantage of energy focusing through time-reversal pulse shaping. Although the peak values in Fig. 11 are lower by roughly 10 times below those of Fig. 10, the focused TR-PPM peaks still clearly convey the transmitted binary data. Hence, TR-PPM method allows signal transmission at substantially reduced SNR conditions.

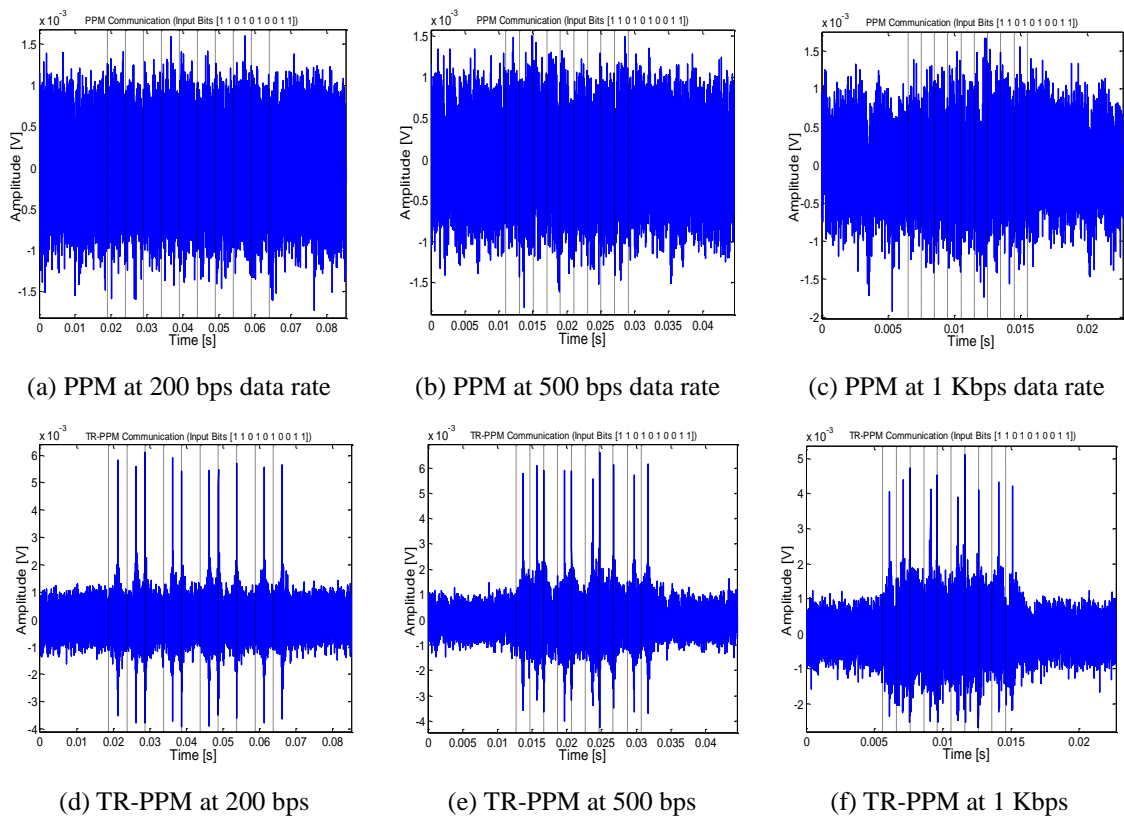


Fig. 13 PPM and TR- PPM communication between SA2 and SA3 in low SNR with bit stream [1101010011]

5.3 Long distance stress wave communication experiments via PPM and TR-PPM

Figs. 14 and 15 shows the received pulse focusing waveform and the received waveform at data rates of 200 bps, 500 bps and 1 Kbps between the farthest SA pairs (i.e., SA1 and SA5). The maximum amplitude of excitation signal is 500 V. Compared with Fig. 9, the focused peaks between SA1 and SA5 (shown in Fig. 14) become wider than those between SA2 and SA3. This is because of the substantial signal attenuation at longer distance and the weakened multipath signal strength, since time reversal techniques achieve signal focusing by using energy from all paths. Also, background noise becomes relatively stronger to degrade the received signal energy quality due to the weaker signal strength through longer distance.

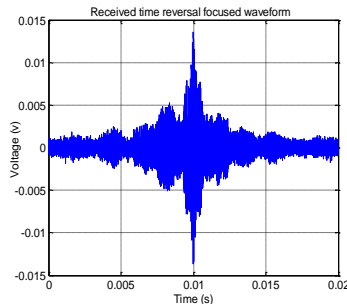


Fig.14 Received time reversal focused waveform (SA1, SA5)

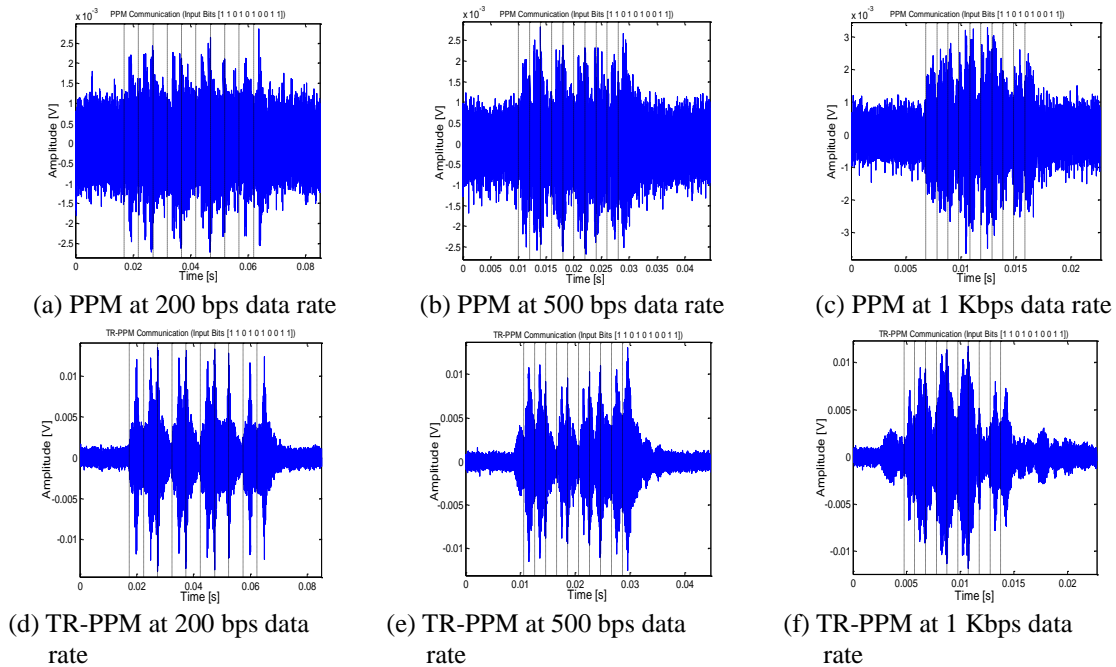


Fig. 15 PPM and TR- PPM communication between SA1 and SA5 with bit stream [1101010011]

We find the received PPM signal peaks become difficult to detection under all three different transmission rates. For TR-PPM, the peaks clearly convey the stream of binary data at 200 bps. When the transmission data rate increases to 500 bps or 1 kbps, the peaks starts to widen and overlap and become less distinguishable because of the relatively longer channel delay spread versus the modulated pulse interval. Although it is expected for achievable transmission rate to drop as transmission distance groups, TR-PPM maintains its performance edge over the traditional PPM.

5. Conclusions

In this paper, we studied marble-based SA pairs as actuator and sensor for transmitting and receiving encoded binary data information over concrete channels. We show that the received stress wave signal encounters severe channel dispersion when using conventional PPM and often becomes difficult to detect. We introduce a time reversal technique for PPM (TR-PPM) that can focus pulsed waves through inhomogeneous multipath channels by utilizing the scattering of waves. Compared with PPM communication, TR-PPM substantially improves data rate, transmission distance, and is robust at lower SNR environment. This work further provides a foundation for future implementation of MIMO stress wave communication links in concrete channels.

Acknowledgments

The authors are grateful to Dr. Peng Li for assisting with SA integrated system testing, analysis of the concrete communication channel, and also for providing suggestions and expertise on conducting the communication experiments in concrete. This material is based upon work supported by NSF awards (CNS-0832089, CCSS-CPS1101547 and CCSS-CPS1102195).

References

- Bocchini, P., Marzani, A. and Viola, E. (2011), "Graphical user interface for guided acoustic waves", *J. Comput. Civil Eng.*, **25**(3), 202-210.
- Edelmann, G., Song, H., Kim S., Hodgkiss, W., Kuperman, W. and Akal, T. (2005), "Underwater acoustic communication using time reversal", *IEEE J. Ocean. Eng.*, **30**(4), 852-864.
- Graham, D., Neasham, J. and Sharif, B. (2009). "High bit rate communication through metallic structures using electromagnetic acoustic transducers", *OCEANS 2009-EUROPE*, 1-6.
- Gu, H., Song G., Dhonde H., Mo Y.L. and Yan S. (2006), "Concrete early-age strength monitoring using embedded piezoelectric transducers", *Smart Mater. Struct.*, **15**(6), 1837-1845.
- Hoult, N.A., Fidler, P.R.A. and Middleton, C.R. (2009), "Wireless structural health monitoring of bridges: current challenges and future innovations", *Proceedings of the 7th AustRoads Bridge Conference*.
- Hou, S., Zhang, H.B. and Ou, J.P. (2012), "A PZT-based smart aggregate for compressive seismic stress monitoring", *Smart Mater. Struct.*, **21**(10), 105035, 1-9.
- Johnson, C.C. (1972), *A seismic communications investigation employing a piezoelectric transducer*.
- Jin, Y., Zhao, D. and Ying, Y. (2011), "Time reversal data communications on pipes using guided elastic waves - Part I: Basic principles", *Proceedings of the SPIE: Smart Structures/NDE Conference*.
- Jin, Y., Ying, Y. and Zhao, D. (2011), "Time reversal data communications on pipes using guided elastic

- waves - Part II: Experimental studies”, *Proceedings of the SPIE: Smart Structures/NDE*, 1-11.
- Jin, Y., Jiang, Y. and Moura, J.M.F. (2007), “Multiple antenna time reversal transmission in ultra-wideband communications”, *Proceedings of the IEEE Globe Communication Conference*.
- Kokossalakis, G. (2006), *Acoustic data communication system for in-pipe wireless sensor network*, PhD Dissertation, Massachusetts Institute of Technology, Cambridge, MA.
- Kailaswar, S., Zheng, R., Kovitz, J., Phung, Q., Wang, H., Ding, Z. and Song, G. (2012), “ConcreteCom: A New Communication Paradigm for Building Structural Health Monitoring”, *Proceedings of the 4th ACM Workshop on Embedded Sensing Systems for Energy-Efficiency in Buildings*.
- Li, P., Gu, H., Song, G., Zheng, R. and Mo, Y.L. (2010), “Concrete structural health monitoring using piezoceramic-based wireless sensor networks”, *Smart Struct. Syst.*, **6**(5-6), 731-748.
- Li, P., Olmi, C. and Song, G. (2010), “Energy efficient wireless sensor network for structural health monitoring using distributed embedded piezoelectric transducers”, *Proceedings of the SPIE: Smart Structures and Materials+ Nondestructive Evaluation and Health Monitoring*, International Society for Optics and Photonics.
- Murphy, T. (2006), *Ultrasonic digital communication system for a steel wall multipath channel: methods and results*, Master's Dissertation, Rensselaer Polytechnic Institute.
- Primerano, R.A. (2010), *High Bit-rate Digital Communication through Metal Channels*, Ph.D. Dissertation, Drexel University, Philadelphia.
- Ramirez-Iniguez, R., Idrus, S.M. and Sun, Z. (2008), *Optical Wireless Communications: IR for Wireless Connectivity*, Boca Raton: CRC Press, USA.
- Song, G., Gu, H. and Mo, Y.L. (2008), “Smart aggregates: multi-functional sensors for concrete structures—a tutorial and a review”, *Smart Mater. Struct.*, **17**(3), 1-17.
- Sharony, J. (2006), *Introduction to Wireless MIMO—Theory and Applications*, CEWIT—Center of Excellence in Wireless and Informational Technology, Stony Brook University, IEEE LI.
- Ying, Y., Soibelman, L., Garrett, J., Jin, Y., Moura, J., Oppenheim, I., O’Donoghue, N. and Harley, J. (2010). “Time reversal detection in pipes”, *Proceedings of the SPIE: Smart Structures/NDT*, 7647, 76473S-1-12.